Anisotropy as a signature of transverse collective flow

Jean-Yves Ollitrault
Service de Physique Théorique, Centre d'Études de Saclay, F-91191 Gif-sur-Yvette CEDEX, France
(Received 19 February 1992)

We show that anisotropies in transverse-momentum distributions provide an unambiguous signature of transverse collective flow in ultrarelativistic nucleus-nucleus collisions. We define a measure of the anisotropy from experimental observables. The anisotropy coming from collective effects is estimated quantitatively using a hydrodynamical model, and compared to the anisotropy originating from finite multiplicity fluctuations. We conclude that collective behavior could be seen in Pb-Pb collisions if a few hundred particle momenta were measured in a central event.

PACS number(s): 25.75.+r, 12.38.Mh, 24.60.Ky, 47.75.+f

I. INTRODUCTION

It is a crucial issue in ultrarelativistic heavy-ion collisions whether or not thermal equilibrium is achieved during the collision. If thermalization occurs, collective effects should play an important role in the subsequent evolution of the system. They have been sought for in transverse-momentum distributions, but no definite conclusion has been drawn so far. In this paper, we propose a signature of transverse collective flow based on a global event-by-event analysis. The same type of analysis has been carried out to test hydrodynamic behavior at lower energies [1]: from the measured final momenta, one constructs the kinetic-energy flow tensor or sphericity tensor. The eigenvector associated with the largest eigenvalue of this tensor corresponds to the direction of maximum energy flow, and its angle with the collision axis is called the flow angle. A correlation is seen experimentally between the flow angle and the multiplicity [2] (or, equivalently, the impact parameter) which is interpreted as coming from collective flow. In this article, we show that a suitably modified sphericity tensor analysis is still relevant at ultrarelativistic energies.

In Sec. II, we recall briefly the definition and the main properties of the usual sphericity tensor. We then consider the ultrarelativistic limit and show that only the transverse components of the sphericity tensor must be taken into account. From these transverse components, we define an index α characterizing the anisotropy of transverse-momentum distributions. We show that collective flow gives rise to a nonvanishing value of this index α for peripheral collisions, and that the correlation of α with impact parameter should thus provide a signature of collective effects. In Sec. III, we give a general discussion of finite multiplicity fluctuations which also produce anisotropy, and thus may mask collective effects. The three following sections are devoted to a quantitative study of how much anisotropy we should expect if collective flow is present. For this purpose, we use a hydrodynamical model to describe the collision. This is briefly described in Sec. IV, where we also show how to calculate anisotropy from the results of hydrodynamics. A crucial ingredient in hydrodynamics is the equation of state. That of hadronic matter is poorly known at temperatures $100 < T < 300$ MeV, and we therefore consider various parametrizations. First we study the simplest case, namely, a massless, noninteracting pion gas (Sec. V). Using a two-dimensional hydrodynamical code, we compute the anisotropy index α as a function of impact parameter for given colliding nuclei. We discuss the effects of changing the parameters of the model (thermalization time and decoupling temperature), and consider various colliding systems. In Sec. VI, we use other equations of state to study how our results are affected by a change in the speed of sound, and to study the effect of a phase transition from a quark-gluon plasma. Finally, in Sec. VII, we discuss under what experimental conditions the anisotropy coming from collective behavior can be disentangled from that coming from finite multiplicity fluctuations.

II. SPHERICITY TENSOR ANALYSIS AT ULTRARELATIVISTIC ENERGIES

A. Situation at low energy

Let us recall the main features of the analysis performed at lower energies [1]. From the measured momenta $\mathbf{p}(\nu)$, $\nu=1,\ldots,M$ in a given collision with multiplicity M, one constructs the sphericity tensor defined in the center-of-mass frame as

$$S_{ij}=\sum_{\nu=1}^{M} w(\nu)p_i(\nu)p_j(\nu)\ , \tag{2.1}$$

where p_i $(i=1,2,3)$ is the ith component of the momentum, and $w(\nu)=1/2m_\nu$ is a weight chosen in such a way that S_{ii} is the total kinetic energy in the nonrelativistic limit. The coordinate system is taken such that z is the collision axis. The tensor S_{ij} contains six independent quantities, which correspond to the three eigenvalues f_1, f_2, f_3 and to three Euler angles specifying the orientation of the three orthogonal eigenvectors. However, as we are going to show, only three parameters are relevant to the flow analysis, which are the flow angle θ_F and the eigenvalue ratios f_1/f_2 and f_1/f_3.

For spherical nuclei, the colliding system is symmetric under reflections with respect to the reaction plane defined by the impact parameter and the collision axis. If statistical fluctuations are neglected, i.e., in the limit of an infinite multiplicity M, S_{ij} has the same symmetry. Then the direction orthogonal to the reaction plane is an eigenvector of S_{ij}. Thus, S_{ij} has an eigenvector perpendicular to the collision axis. This property allows, in fact, the construction of the reaction plane from S_{ij}: it is defined as the plane orthogonal to the eigenvector of S_{ij} which is perpendicular to the collision axis z. The constraint that one of the three eigenvectors of S_{ij} is perpendicular to the z axis eliminates one of the angular degrees of freedom. This constraint can written explicitly as

$$S_{13}S_{23}(S_{11}-S_{22})-S_{12}(S_{13}^2-S_{23}^2)=0 . \tag{2.2}$$

Now, through a rotation about the collision axis z, we can choose the x axis in such a way that (x,z) is the reaction plane (x is then the direction of impact parameter). This eliminates one more irrelevant parameter, corresponding to the azimuthal angle of the reaction plane. Then there is only one relevant angle left. We denote by f_2 the eigenvalue corresponding to the y axis, and label the two other eigenvalues so that $f_1 \le f_3$. We then define the flow angle θ_F as the angle between the collision axis and the eigenvector associated with f_3. θ_F lies between 0 and $\pi/2$, and the matrix of the sphericity tensor reads

$$S=\begin{pmatrix} f_1\cos^2\theta_F+f_3\sin^2\theta_F & 0 & 2(f_3-f_1)\sin\theta_F\cos\theta_F \\ 0 & f_2 & 0 \\ 2(f_3-f_1)\sin\theta_F\cos\theta_F & 0 & f_1\sin^2\theta_F+f_3\cos^2\theta_F \end{pmatrix} . \tag{2.3}$$

We are left with three relevant dimensionless parameters, which are, for instance, the flow angle θ_F and the eigenvalue ratios f_1/f_2 and f_1/f_3, various combinations of which have been considered in the literature [3], such as sphericity, flatness, etc.

We have neglected statistical fluctuations so far. Fluctuations are irrelevant to the flow analysis, which is essentially a macroscopic description, but they are present in the experiment where a finite number of particles is seen. Thus, the particle distribution is not strictly symmetric with respect to the reaction plane and none of the eigenvectors of S_{ij} is strictly orthogonal to the collision axis. Then, the definition of θ_F according to the above discussion is ambiguous. For this reason, θ_F is defined experimentally as the angle of the largest principal axis of S_{ij} with the collision axis. This is consistent with the previous definition if f_3 is the largest eigenvalue, that is, if $f_2 \le f_3$ (since we have chosen $f_1 \le f_3$), which is a reasonable assumption: $f_2 > f_3$ would mean that the maximum kinetic-energy flow is orthogonal to the reaction plane, which seems very unlikely.

The correlation between θ_F and the multiplicity (which is itself correlated to the impact parameter) has been the most studied one. At low energies, fluid dynamical models predict that θ_F increases from 0 for peripheral collisions to 90° for central collisions [3]. Note that for central collisions azimuthal symmetry alone implies that either $f_1=f_2<f_3$ and $\theta_F=0$, or $f_1<f_2=f_3$ and $\theta_F=90°$. Thus, $\theta_F=90°$ simply means that most of the energy goes into the transverse directions, while $\theta_F=0$ would mean that most of the energy remains in the longitudinal direction. Since θ_F may take only two values, it clearly does not vary continuously with the sphericity tensor, and its definition is ambiguous for a spherical event ($f_1=f_2=f_3$) where the discontinuity occurs. However, this discontinuity is smoothed off by finite multiplicity fluctuations, which cause considerable deviations from the fluid dynamical value for near-spherical events. It is therefore questionable whether θ_F is the best quantity to consider. However, the predicted increase of θ_F with the multiplicity is indeed seen experimentally [2] (although it does not reach $\theta_F=90°$ due to fluctuations, as expected), indicating the presence of collective flow at low energies.

B. Ultrarelativistic limit

Now, what happens at ultrarelativistic energies? Because of nuclear transparency, most of the available energy remains in the longitudinal direction: In the center-of-mass frame, the typical transverse momenta are of the order of a few hundred MeV, while the longitudinal momenta can be of the same order of magnitude as the initial ones, that is a few GeV at CERN energies. Thus, the energy flows principally in the longitudinal direction, and one expects $\theta_F \to 0$ and $f_1, f_2 \ll f_3$ as the incident energy increases, independently of whether or not there are collective effects. In other terms, the nuclei do not bounce off significantly, and thus θ_F and f_3 become irrelevant parameters at ultrarelativistic energies.

However, transverse collective flow may occur in the colliding system among the produced particles, and it may affect the sphericity tensor. To see this, consider a peripheral collision, such as schematically depicted in Fig. 1, and consider the matter produced in the central rapidity region. If the collision can be viewed as a superposition of a large number of independent nucleon-nucleon collisions, that is, if no collective behavior takes place, the momentum distribution is isotropic in the transverse plane. If, on the other hand, a thermal equilibrium is reached, the pressure gradient is directed mainly along the direction of the impact parameter, and a collective flow develops in this direction according to the Euler equation of fluid dynamics. This, in turn, reflects itself in the transverse momenta which are also preferentially oriented along the same line. Let us emphasize that this anisotropy in momentum distributions need not be present in the initial state of the collision, when the particles are formed. It is only the spatial distribution which is initially anisotropic for nonzero impact parameter, and this anisotropy is carried over to the momentum distributions through pressure gradient.

Now, let us see how this sidesplash of the reaction products reflects itself in the sphericity tensor. Consider the restriction of S_{ij} to the transverse plane (x,y) in the limit $\theta_F \to 0$, $f_3 \to \infty$. Equation (2.3) becomes

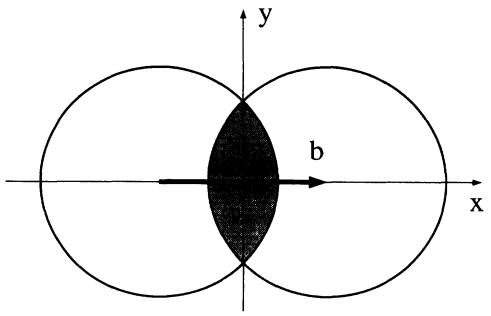

FIG. 1. Peripheral collision viewed in the transverse plane. **b** is the impact parameter. The shaded area corresponds to the region where particles are created in the central rapidity region. Outside this region is the vacuum.

$$S^{\perp}=\begin{bmatrix} f_1+f_3\theta_F^2 & 0 \\ 0 & f_2 \end{bmatrix} . \tag{2.4}$$

The term $f_3\theta_F^2$, which may be important, is the remnant of the bounce off. From Eq. (2.3), one gets $f_3 \simeq S_{33}=\sum_{\nu=1}^{M} w(\nu)p_z^2(\nu)$. Thus, the main contribution to f_3 comes from the fragmentation regions which correspond to the highest values of $|p_z|$ in the center-of-mass frame. We shall hereafter restrict our study to the central rapidity region where $|p_z|$ is much smaller, and we assume that $f_3\theta_F^2$ is negligible in this case. Then $f_1 \simeq S_{11}=\sum_{\nu=1}^{M} w(\nu)p_x^2(\nu)$, $f_2=S_{22}=\sum_{\nu=1}^{M} w(\nu)p_y^2(\nu)$, and the sidesplash of the reaction products along the direction of impact parameter x results in $f_1>f_2$. The whole rapidity range may contribute to this effect. A natural measure of this anisotropy in transverse momenta is the dimensionless observable α defined as

$$\alpha=\frac{f_1-f_2}{f_1+f_2}=\frac{\sum_{\nu=1}^{M} w(\nu)[p_x(\nu)^2-p_y(\nu)^2]}{\sum_{\nu=1}^{M} w(\nu)[p_x(\nu)^2+p_y(\nu)^2]} . \tag{2.5}$$

$\alpha=0$ for an isotropic distribution ($f_1=f_2$), whereas $\alpha=1$ if all momenta are directed along the impact line ($f_2=0$). The last equality in Eq. (2.5) holds only if x is the direction of impact parameter. Alternatively, we can use the following expression which is valid in any coordinate system for the transverse plane:

$$\alpha=\left[1-\frac{4\det S^{\perp}}{(\mathrm{tr}S^{\perp})^2}\right]^{1/2} . \tag{2.6}$$

This allows one to calculate α directly as a function of the measured transverse sphericity tensor $S_{ij}^{\perp}$. It appears clearly in this form that α is the only observable we can construct from $S_{ij}^{\perp}$ if we require it to be dimensionless and invariant through rotations about the collision axis. The ultrarelativistic case is thus simpler than the low-energy case where three rotationally invariant and dimensionless parameters must be considered. A collective flow would reveal itself through a nonzero value of α for peripheral collisions, while $\alpha=0$ for central collisions, which are isotropic in the transverse plane. So we must study the correlation of α with the multiplicity (we recall that the multiplicity is a fair measure of the impact parameter [4]). We expect that α will be a decreasing function of the multiplicity if collective transverse flow occurs.

Finally, note that the weight $w(\nu)=1/2m_{\nu}$ in Eq. (2.1) is quite inappropriate at ultrarelativistic energies. First, S_{ii} does not represent the kinetic energy any more. Second, composite fragments for which this weight was introduced represent a negligible fraction of the emitted particles, especially in the central rapidity region. Third, the transverse momenta of different types of particles have comparable distributions (this is the observed m_T scaling [5]). Thus, we shall take $w(\nu)=1$, and the transverse sphericity tensor is then simply defined as

$$S_{ij}^{\perp}=\sum_{\nu=1}^{M} p_i(\nu)p_j(\nu) \tag{2.7}$$

with $i,j=1,2$. Since $S_{ij}^{\perp}$ only involves the transverse momenta, it is invariant under Lorentz boosts along the collision axis. This is a nice property from a theoretical point of view since the central rapidity region is expected to enjoy the same property at high energies [6]. From the experimental point of view, restricting ourselves to transverse coordinates allows us to measure $S_{ij}^{\perp}$ directly in the laboratory frame for fixed-target experiments.

III. FINITE MULTIPLICITY FLUCTUATIONS

A. Jacobian-free analysis

With a finite number of particles M, one never obtains an isotropic distribution, even if the particles are emitted according to an isotropic emission probability. Even worse, as we shall see, an isotropic emission probability gives rise to a probability law for α which is not centered at $\alpha=0$ as we would expect, but rather at a value $\alpha \sim 1/\sqrt{M}$. Here we show how to get rid of this shift by defining a corrected distribution for α, following the analysis of Danielewicz and Gyulassy [7].

If correlations between particles are neglected, the central limit theorem states that in the limit of large multiplicity M the probability law for $S_{ij}^{\perp}$ is of Gaussian form and strongly peaked around its mean value $\langle S_{ij}^{\perp} \rangle$, with a width varying like $1/\sqrt{M}$. However, we are not interested in the distribution of $S_{ij}^{\perp}$ but rather in the distribution of α. In order to change variables, we need two other quantities since $S_{ij}^{\perp}$ has three independent components. We take, for instance, $\mathcal{E} \equiv \mathrm{tr}S^{\perp}=\sum_{\nu=1}^{M} p_T^2(\nu)$ and the angle θ between the x axis and the largest principal axis of $S_{ij}^{\perp}$. Then, in terms of the variables $(\alpha,\mathcal{E},\theta)$, the expression of $S^{\perp}$ is

$$S^{\perp}=\frac{\mathcal{E}}{2}\begin{bmatrix} 1+\alpha\cos 2\theta & \alpha\sin 2\theta \\ \alpha\sin 2\theta & 1-\alpha\cos 2\theta \end{bmatrix} . \tag{3.1}$$

Transforming variables from $S_{ij}^{\perp}$ to α, $\mathcal{E}$, and θ brings in a Jacobian factor

$$J(\alpha,\theta,\mathcal{E})=\frac{\partial(S_{11},S_{12},S_{22})}{\partial(\alpha,\theta,\mathcal{E})}=\alpha\mathcal{E}^2 . \tag{3.2}$$

The fact that this Jacobian is proportional to α expresses that the probability to generate an isotropic event vanishes: therefore, the maximum of the probability distribution is at $\alpha\neq 0$, even for an isotropic emission. In order to define a clear signature for anisotropy, this distortion must be eliminated. This can be done simply by dividing the probability distribution $dP/d\alpha\, d\theta\, d\mathcal{E}$ by the Jacobian. Since $\mathcal{E}=\sum_{\nu=1}^{M} p_T^2(\nu)$, the central limit theorem ensures that the fluctuation of $\mathcal{E}$ around its average value $\bar{\mathcal{E}}=M\langle p_T^2\rangle$ is small. Therefore, we omit the factor $\mathcal{E}^2$ in Eq. (3.2). Integrating over θ and $\mathcal{E}$, we thus define a corrected distribution for α:

$$\frac{dP_{\rm cor}}{d\alpha}=\frac{1}{\alpha}\frac{dP}{d\alpha} , \tag{3.3}$$

where $dP/d\alpha$ is the true distribution. While the true distribution always vanishes for $\alpha=0$, we show in Appendix A that the corrected distribution is maximal at $\alpha=0$ if the emission law is isotropic. More precisely, for an uncorrelated, isotropic emission law, the corrected distribution for α is Gaussian in the limit of large M:

$$\frac{dP_{\rm cor}}{d\alpha}\propto \exp\left[-\frac{M\alpha^2}{\delta}\right] , \tag{3.4}$$

where $\delta=\langle p_T^4\rangle/\langle p_T^2\rangle^2$. Equation (3.4) is important: first, it shows that statistical fluctuations for α are of order $1/\sqrt{M}$; second, it illustrates the usefulness of the Jacobian correction (the uncorrected distribution would reach its maximum at $\alpha=\sqrt{\delta/2M}$); third, it proves that a peak at $\alpha\neq 0$ in the corrected distributions can be safely interpreted as due to some anisotropy in the emission probability. Let us finally comment on the parameter δ, through which the momentum distribution comes into play: a quick calculation shows that $\delta=2$ for a Gaussian distribution, while $\delta=\frac{10}{3}$ for an exponential distribution. Since the width of the Gaussian in Eq. (3.4) is proportional to $\sqrt{\delta}$, the finite multiplicity fluctuations for α are somewhat larger with an exponential p_T distribution than with a Gaussian p_T distribution.

B. Explicit calculation with a Gaussian parametrization

We have shown that a peak at $\alpha\neq 0$ in the corrected probability means that there is anisotropy in the emission probability itself. We now study whether the converse statement is true, that is, under what conditions the anisotropy in the emission probability results in a peak of the corrected distribution at $\alpha\neq 0$. In this section, we consider a very simple model where the emission is uncorrelated and the transverse-momentum distribution is Gaussian. The distribution $dP_{\rm cor}/d\alpha$ can then be calculated exactly for any M. More general results, which are valid for an arbitrary momentum distribution but only in the limit of large M, are derived in Appendix A.

Following Danielewicz and Gyulassy [7] again, we take a probability distribution for the M transverse momenta of the form

$$\frac{dP}{d^2p_T(1)\cdots d^2p_T(M)}\propto \exp\left[\frac{-M}{2}\,\mathrm{tr}(S^{\perp}\bar{S}^{-1})\right] , \tag{3.5}$$

where $S^{\perp}$ is the transverse sphericity tensor defined by Eq. (2.7) and $\bar{S}$ is the average value of $S^{\perp}$; its coefficients are given by $\bar{S}_{ij}=M\langle p_i p_j\rangle$. Choosing the coordinate axes in such a way that $\bar{S}_{12}=0$ and $S_{11}>S_{22}$, one can write $\bar{S}$ in the form

$$\bar{S}=(\bar{\mathcal{E}}/2)\,\mathrm{diag}(1+\bar{\alpha},1-\bar{\alpha}) \tag{3.6}$$

[compare with Eq. (3.1)], where $\bar{\mathcal{E}}=M\langle p_T^2\rangle$ and $\bar{\alpha}=(\langle p_x^2\rangle-\langle p_y^2\rangle)/(\langle p_x^2\rangle+\langle p_y^2\rangle)$ represents the anisotropy associated with $\bar{S}$, as defined by Eq. (2.5) or Eq. (2.6), i.e., the anisotropy in the emission probability. The probability distribution (3.5) can be written as a product of one-particle probabilities using Eq. (2.7) and is therefore uncorrelated. The probability law for $S^{\perp}$ can be calculated from Eq. (3.5):

$$\frac{dP}{dS_{11}^{\perp}\,dS_{12}^{\perp}\,dS_{22}^{\perp}}\propto(\det S^{\perp})^{(M-3)/2}\exp\left[\frac{-M}{2}\,\mathrm{tr}(S^{\perp}\bar{S}^{-1})\right] . \tag{3.7}$$

It is of Gaussian form for $M\gg 1$ [7]. In terms of the variables $(\alpha,\theta,\mathcal{E})$, Eq. (3.7) becomes, using Eqs. (3.1) and (3.2),

$$\frac{dP}{d\alpha\, d\theta\, d\mathcal{E}}\propto\alpha(1-\alpha^2)^{(M-3)/2}\mathcal{E}^{M-1}\times\exp\left[-\frac{M\mathcal{E}}{\bar{\mathcal{E}}}\,\frac{1-\alpha\bar{\alpha}\cos 2\theta}{1-\bar{\alpha}^2}\right] . \tag{3.8}$$

Integration over $\mathcal{E}$ yields immediately

$$\frac{dP}{d\alpha\, d\theta}\propto\alpha(1-\alpha^2)^{(M-3)/2}(1-\alpha\bar{\alpha}\cos 2\theta)^{-M} . \tag{3.9}$$

In the case of an isotropic emission law, $\bar{\alpha}=0$. The integration over θ is then trivial and the corrected distribution for α reads

$$\frac{dP_{\rm cor}}{d\alpha}\propto(1-\alpha^2)^{(M-3)/2} . \tag{3.10}$$

In the limit of large M this becomes

$$\frac{dP_{\rm cor}}{d\alpha}\propto\exp\left[-\frac{M\alpha^2}{2}\right] \tag{3.11}$$

in agreement with Eq. (3.4) since $\delta=2$ for a Gaussian p_T distribution.

Consider now the case when the emission law is not isotropic; that is, when $\bar{\alpha}\neq 0$. In the limit of large M, one naturally expects that the corrected probability distribution has a well-defined peak at $\alpha=\bar{\alpha}$. Since the statistical fluctuations for α are of order $1/\sqrt{M}$, one further expects this to be true if $\bar{\alpha}\gg 1/\sqrt{M}$. Indeed, when $\bar{\alpha}\gg 1/\sqrt{M}$, the integral of Eq. (3.9) over θ can be evaluated using a saddle-point approximation, and one obtains

$$\frac{dP_{\rm cor}}{d\alpha} \propto \exp\left[-\frac{M}{2}\left[\frac{\alpha-\bar{\alpha}}{1-\bar{\alpha}^2}\right]^2\right], \tag{3.12}$$

which is a Gaussian of width $(1-\bar{\alpha}^2)/\sqrt{M}$, centered at $\alpha=\bar{\alpha}$ as expected. But let us now see what happens when $\bar{\alpha}\sim 1/\sqrt{M}$. The integral of Eq. (3.9) over θ can be done analytically, which yields the following exact expression for the corrected distribution:

$$\frac{dP_{\rm cor}}{d\alpha} \propto (1-\alpha^2)^{(M-3)/2}\frac{1}{\sqrt{1-\alpha^2\bar{\alpha}^2}} \times \sum_{k=0}^{M-1}\frac{(2M-2k-3)!!}{(M-k-1)!}\frac{(2k-1)!!}{k!} \times \frac{1}{(1+\alpha\bar{\alpha})^{M-1-k}(1-\alpha\bar{\alpha})^k}. \tag{3.13}$$

Figure 2 displays $dP_{\rm cor}/d\alpha$ for $\bar{\alpha}=0.2$ and three different values of M. The Gaussian defined by Eq. (3.12) is close to the exact curve for $M=200$. On the other hand, if $M=40$, $dP_{\rm cor}/d\alpha$ does not look like a Gaussian centered at $\alpha=\bar{\alpha}$. Instead, it is maximal for $\alpha=0$. This means that no maximum at $\alpha\neq 0$ reveals the anisotropy present in the emission law if $M=40$; thus, the corrected distribution (3.3) is not a panacea against finite multiplicity effects. The condition under which the maximum lies at $\alpha\neq 0$ can be derived simply by expanding Eq. (3.9) to order α^2 and then integrating over θ. One gets

$$\bar{\alpha} > \left[\frac{2(M-3)}{M(M+1)}\right]^{1/2} \underset{M\to\infty}{\sim} \left[\frac{2}{M}\right]^{1/2}. \tag{3.14}$$

Equation (3.14) can be understood simply: there is a maximum of the corrected probability distribution at $\alpha\neq 0$ if $\bar{\alpha}$ is greater than the statistical fluctuations which are of order $1/\sqrt{M}$. For the value $\bar{\alpha}=0.2$, which corresponds to Fig. 2, condition (3.14) is satisfied only for $M>45$.

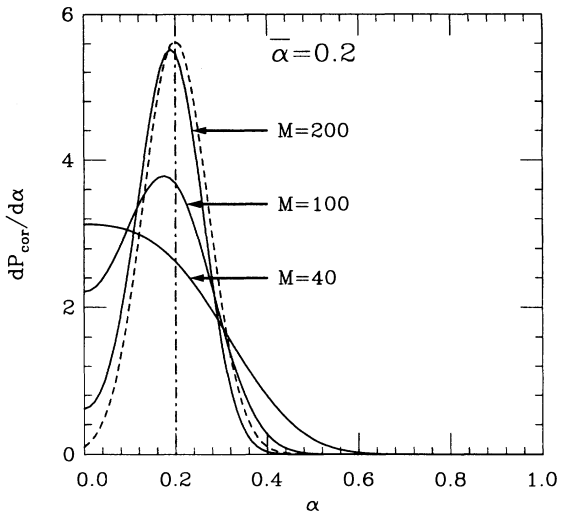

FIG. 2. Solid lines: corrected probability distributions of α calculated according to Eq. (3.13) with $\bar{\alpha}=0.2$ and $M=40$, 100, or 200. The normalization has been chosen such that $\int_0^1 (dP_{\rm cor}/d\alpha)d\alpha=1$. Dashed line: Gaussian approximation (3.12) for $M=200$.

Equation (3.14) can be regarded as a condition for the anisotropy to be observable experimentally. It may be somewhat too pessimistic in the sense that the probability distributions for $\bar{\alpha}=0$ and $\bar{\alpha}\neq 0$ differ, even if both are maximal at $\alpha=0$. Equation (3.14) may also be too optimistic for two reasons: The first is that we have considered a Gaussian distribution and the discussion following Eq. (3.4) shows that finite multiplicity effects are larger for an exponential distribution (we recall that the observed p_T distributions are rather close to exponentials). The generalization of Eq. (3.14) for an arbitrary uncorrelated distribution is, in fact,

$$\bar{\alpha} > \sqrt{\delta/M} \tag{3.15}$$

for large M. This is demonstrated in Appendix A. The second reason why Eq. (3.14) may be too optimistic is that we have totally neglected correlations, which decrease the number of independent sources and therefore increase finite multiplicity fluctuations. However, we expect the general idea to be more or less model independent: the anisotropy $\bar{\alpha}$ present in the emission law can be seen experimentally only if the number M of measured momenta in a single event is at least of order $1/\bar{\alpha}^2$.

IV. ANISOTROPY AND HYDRODYNAMICS

The question that naturally arises now is: What value of $\bar{\alpha}$ should we expect if collective effects are present? In order to estimate this effect, we use a hydrodynamical model [6,8–10] to describe the colliding system. One assumes that the latter behaves as a perfect fluid during some stage of its evolution. Its evolution is then ruled by the equations of relativistic hydrodynamics. The time when hydrodynamical behavior starts is the time at which the system thermalizes; this initial time, which is measured from the beginning of the collision, will be noted t_0. Hydrodynamical expansion lasts until the mean free path of the particles is of the order of the dimensions of the system: one usually assumes that this happens when the temperature decreases down to some decoupling temperature T_d: particles are then emitted freely along the isotherm σ ($T=T_d$), with their momentum distributions given by the state of the fluid at the considered point [11]. $\bar{\alpha}$ is then calculated from these momentum distributions.

A. General formulas from particle distributions

The number of particles of a given type emitted in the phase-space volume d^3p is obtained [11] by integration over the decoupling isotherm σ ($T=T_d$):

$$dN=\int_\sigma p^\mu d\mu(p)d\sigma_\mu, \tag{4.1}$$

where $d\mu(p)$ is the invariant measure defined by

$$d\mu(p)=\frac{\nu_h}{(2\pi)^3}\left[\exp\left[\frac{p^\mu u_\mu}{T_d}\right]-\varepsilon\right]^{-1}\frac{d^3p}{E} \tag{4.2}$$

with $\varepsilon=1$ for bosons and $\varepsilon=-1$ for fermions. In Eq. (4.2), u^μ denotes the fluid four-velocity at the considered point on the isotherm, T_d is the decoupling temperature, and ν_h is the degeneracy factor coming from spin and isospin ($\nu_h=3$ for pions). In this section we assume that all the emitted particles have the same mass and statistics, but our results can be generalized straightforwardly by summing over particle species. We also assume that the central rapidity region is baryon-free, as expected in the high-energy limit; otherwise a chemical potential associated with baryon-number conservation should be present in Eq. (4.2). Note that $E\,d\mu(p)d^3x$ is simply the number of particles in the fluid volume d^3x and in the phase space volume d^3p. With this notation, the sphericity tensor (2.7) can be simply expressed as

$$\bar{S}_{ij}=\int p^i p^j dN=\int_\sigma d\sigma_\mu \int p^i p^j p^\mu d\mu(p)\ . \tag{4.3}$$

We write $\bar{S}_{ij}$ instead of S_{ij} to keep in mind that fluctuations are neglected in hydrodynamics, and Eq. (4.3) is to be understood as an average value. Equation (4.3) shows that the sphericity tensor involves the third moments of the momentum distribution. We thus define the third-rank, completely symmetric tensor

$$S^{\mu\nu\rho}=\int p^\mu p^\nu p^\rho d\mu(p)\ . \tag{4.4}$$

This quantity is calculated in Appendix B. The result is

$$S^{\mu\nu\rho}=Au^\mu u^\nu u^\rho - C(g^{\mu\nu}u^\rho+g^{\nu\rho}u^\mu+g^{\rho\mu}u^\nu) \tag{4.5}$$

with

$$\begin{aligned} A&=(2\langle\langle E^2\rangle\rangle-m^2)n\ ,\\ C&=\frac{\langle\langle E^2\rangle\rangle-m^2}{3}n\ . \end{aligned} \tag{4.6}$$

Thus, the determination of the sphericity tensor reduces to the calculation of $\langle\langle E^2\rangle\rangle$, which denotes the average value of the energy squared E^2 measured in the rest frame of the fluid.

In the case of massless bosons, for instance, the only energy scale is the temperature T and therefore $\langle\langle E^2\rangle\rangle\propto T^2$. The numerical coefficient is calculated by integrating directly over the particle distribution (4.2), which yields

$$\begin{aligned} A&=\frac{24\zeta(5)}{\pi^2}\nu_h T^5\ ,\\ C&=A/6\ , \end{aligned} \tag{4.7}$$

where $\zeta(5)\simeq 1.037$. In the case of massless fermions with zero chemical potential, A must be multiplied by $\frac{15}{16}$. For massive particles, $\langle\langle E^2\rangle\rangle$ must be calculated numerically using Eq. (4.2). A rough estimate is obtained by setting $\langle\langle E^2\rangle\rangle\approx\langle\langle E\rangle\rangle^2=(\epsilon/n)^2$, ϵ being the energy density. This approximation underestimates $\langle\langle E^2\rangle\rangle$. The error, however, vanishes in the nonrelativistic limit; it is maximal for massless particles where $\langle\langle E^2\rangle\rangle\simeq 1.42\langle\langle E\rangle\rangle^2$ (bosons) or $\langle\langle E^2\rangle\rangle\simeq 1.30\langle\langle E\rangle\rangle^2$ (fermions).

There is one point we would like to emphasize before we go any further. In thermodynamics, an equation of state is merely a relation between the entropy density s, the temperature T, and, if any, the chemical potentials μ_i associated with conserved quantities. In a hydrodynamical model, however, we also need to interpret the equation of state in terms of its particle content at decoupling. In doing this, we must make sure that thermodynamic quantities deduced from Eq. (4.1) are consistent with the equation of state, at least at the decoupling temperature. More precisely, one must check that both the energy density $\epsilon(T_d)$ and the pressure $P(T_d)$ match on both sides of the isotherm; otherwise energy and momentum are not conserved at decoupling. For massless particles, for instance, one obtains directly from Eq. (B2) that the equation of state must satisfy $T^\mu_\mu=\epsilon-3P=0$, as is well known for blackbody radiation. Now, the calculation of the sphericity tensor requires the knowledge of $\langle\langle E^2\rangle\rangle$, m, and n, which are not simply related to thermodynamic quantities. Therefore, if we make hydrodynamic calculations with an arbitrary equation of state, we cannot *a priori* define the sphericity tensor as long as the particle content of the equation of state is not explicit.

However, one easily obtains upper and lower bounds on the anisotropy which do not require the knowledge of the particle content. Indeed, from Eq. (4.6) one gets

$$0<C<\frac{A}{6}\ . \tag{4.8}$$

Now, if the x axis is taken along the direction of impact parameter, the anisotropy defined by Eq. (2.5) reads

$$\bar{\alpha}=\frac{\bar{S}_{11}-\bar{S}_{22}}{\bar{S}_{11}+\bar{S}_{22}}=\frac{\langle p_x^2\rangle-\langle p_y^2\rangle}{\langle p_x^2\rangle+\langle p_y^2\rangle}\ . \tag{4.9}$$

Using Eqs. (4.3)–(4.5), this becomes

$$\bar{\alpha}=\frac{A(T_d)\int_\sigma (u_x^2-u_y^2)u^\mu d\sigma_\mu+2C(T_d)\int_\sigma (u^x d\sigma_x-u^y d\sigma_y)}{A(T_d)\int_\sigma (u_x^2+u_y^2)u^\mu d\sigma_\mu+2C(T_d)\int_\sigma (u^\mu d\sigma_\mu+u^x d\sigma_x+u^y d\sigma_y)}\ . \tag{4.10}$$

We have used the fact that $\langle\langle E^2\rangle\rangle$ and thus A and C are functions of the temperature only (since we have assumed that the baryon chemical potential is zero), and therefore factor out on the isotherm σ ($T=T_d$). The variation of $\bar{\alpha}$ with C is clearly monotonous (in all the cases studied in the following sections, $\bar{\alpha}$ decreases with increasing C). Thus, the upper and lower bounds on C in Eq. (4.8) give upper and lower bounds on $\bar{\alpha}$. Of course, this is interesting only if the upper bound and the lower bounds are close to each other. This is the case when the fluid is ultrarelativistic, in the sense that $u^0\gg 1$. Indeed, in this case the term proportional to C in Eq. (4.5) is of order

$(u^0)^{-2}$ times the term proportional to A and can therefore be neglected. Thus, in the limit $u^0 \gg 1$, the upper and lower limit on $\bar{\alpha}$ coincide, and $\bar{\alpha}$ is given by Eq. (4.10) in which we set $C=0$. This value is independent of the particle content of the equation of state. Note that, in the ultrarelativistic limit, the product $u^0 T$ is constant on the trajectory of a fluid element [12]. Thus, the difference between the upper and lower bound on $\bar{\alpha}$, which is of order $(u^0)^{-2}$, varies with the decoupling temperature like T_d^2. For small T_d, the value of α depends little on the particle content of the equation of state. This result will be used in Sec. VI C.

B. A simple example

As an illustration, let us consider the case of a fluid in uniform motion along the x axis with four-velocity $u^\mu \equiv (\sqrt{1+u^2}, u, 0, 0)$. This collective motion clearly introduces some anisotropy in the transverse plane (x,y). From Eqs. (4.4)–(4.6), one gets

$$\begin{aligned} \langle p_x^2 \rangle &= \frac{S^{110}}{nu^0} = \frac{\langle\langle E^2 \rangle\rangle - m^2}{3} + (2\langle\langle E^2 \rangle\rangle - m^2)u^2 , \\ \langle p_y^2 \rangle &= \langle p_z^2 \rangle = \frac{S^{220}}{nu^0} = \frac{\langle\langle E^2 \rangle\rangle - m^2}{3} , \end{aligned} \tag{4.11}$$

where single angular brackets denote average quantities measured in the laboratory frame. In the nonrelativistic limit $T \ll m$, we expect that thermal motion and collective motion give additive contributions to the energy. Indeed, using $\langle\langle E \rangle\rangle \simeq m$ and $\langle\langle p^2/2m \rangle\rangle \simeq 3T/2$ (Boltzmann statistics), the last equation reduces to

$$\begin{aligned} \langle p_x^2 \rangle &= mT + m^2 u^2 , \\ \langle p_y^2 \rangle &= \langle p_z^2 \rangle = mT , \end{aligned} \tag{4.12}$$

as expected. In the ultrarelativistic limit $T \gg m$, on the other hand, Eq. (4.7) can be used and one gets for massless bosons, using $n = [\zeta(3)/\pi^2] \nu_h T^3$,

$$\langle p_T^2 \rangle = \langle p_x^2 \rangle + \langle p_y^2 \rangle = \frac{8\zeta(5)}{\zeta(3)} T^2 (1+3u^2) . \tag{4.13}$$

This result differs from Eq. (5.9) of Ref. [13] by $3u^2 \to \frac{5}{2}u^2$. Note that, in contrast with the nonrelativistic case, thermal and collective motions are not decoupled in Eq. (4.13).

Let us now calculate the anisotropy. Thanks to the $y \to -y$ symmetry, $S_{ij}^{\perp}$ is diagonal and Eq. (4.9) can be used. Using Eq. (4.11), one gets a general expression for $\bar{\alpha}$, which reduces to

$$\bar{\alpha} = \frac{u^2}{u^2 + 2T/m} \tag{4.14}$$

in the nonrelativistic limit and to

$$\bar{\alpha} = \frac{u^2}{u^2 + 1/3} \tag{4.15}$$

in the ultrarelativistic limit $T \gg m$. It is clear on this very simple example that anisotropy measures the relative importance of collective motion and thermal motion: $\bar{\alpha} = 0$ if there is no collective motion, while $\bar{\alpha} \to 1$ for large u.

Finally, let us calculate the upper and lower bounds on $\bar{\alpha}$ derived from Eq. (4.8). The limit $C=0$ corresponds in this case to $\langle p_y^2 \rangle = 0$ [using Eq. (4.4)] which gives $\bar{\alpha} = 1$. In the limit $C = A/6$, on the other hand, $\bar{\alpha}$ is given by Eq. (4.15). As we said in the discussion following Eq. (4.10), the two limits coincide only in the limit $u \gg 1$.

C. Our hydrodynamical model

A hydrodynamical model is entirely specified by the equation of state, the initial conditions, the initial (or thermalization) time t_0, and the decoupling temperature T_d. The initial time t_0 and the decoupling temperature T_d are subject to large uncertainties. Therefore, we do not specify their values here; instead, we shall allow them to vary in the numerical calculations presented in the next section, so as to study the effect of changing these parameters. The model we use, which is described in detail in [10], makes two general assumptions. The first is that the central rapidity region is baryonless. Then there is *a priori* no conserved quantity, and thermodynamic quantities are functions of one thermodynamic parameter only, for instance, the temperature T; the equation of state is entirely determined by the behavior of the entropy density s as a function of T. Several parametrizations will be used in Secs. V and VI. The second assumption is that the central rapidity is invariant under Lorentz boosts in the longitudinal direction, and that the longitudinal fluid velocity satisfies Bjorken's scaling law [6]: $v_z = z/t$. This allows one to get rid of the longitudinal direction z in the numerical calculations. The equations of hydrodynamics are then solved numerically using the two-dimensional code described in [12].

Let us now briefly discuss our initial conditions. According to our hypotheses, they are longitudinally boost invariant so we only need to specify them in the transverse plane. Since the nucleon-nucleon collisions that create matter in the central rapidity region have no preferred direction in the transverse plane, the initial transverse velocity of the fluid must be zero. Furthermore, since there is only one thermodynamic parameter in our equation of state, the initial conditions are entirely specified by, for instance, the initial entropy density. We assume that the entropy density at a point in the transverse plane is proportional to the density of participant nucleons at that point. The latter quantity is calculated in the framework of the Glauber model using a standard parametrization of the nuclear density, as in [14]:

$$\rho(r) = \rho_0 / \{1 + \exp[(r-c)/\xi]\} , \tag{4.16}$$

where $c \simeq 1.08 A^{1/3}$ fm is the half-density radius, $\xi \simeq 0.55$ fm is proportional to the skin thickness, and ρ_0 is a normalization constant. Let T_A and T_B denote the profile functions of the target and projectile nuclei, respectively $[T(\mathbf{r}) = \int \rho(\sqrt{r^2+z^2}) dz]$. The density of participants at a point $\mathbf{r}$ in the transverse plane is then given by [15]

$$\frac{dN_A}{d^2 r} = T_A(\mathbf{r}) \left[1 - \left[1 - \frac{\sigma_{\text{in}} T_B(\mathbf{r}-\mathbf{b})}{B} \right]^B \right] \tag{4.17}$$

for the target nucleus, and a similar formula with A and B exchanged for the projectile nucleus. In Eq. (4.17), **b** is the impact parameter and $\sigma_{in} \simeq 33$ mb is the total inelastic nucleon-nucleon cross section The initial entropy density is then taken proportional to the total density of participants: $s_0 \propto dN_A/d^2r + dN_B/d^2r$. The proportionality constant is chosen in such a way that the final multiplicity corresponds to the experimental value. At CERN energies, the multiplicity per unit rapidity and per participant is approximately 2. This is the value we take in the numerical calculations presented in the following sections. At energies to be reached at the BNL Relativistic Heavy Ion Collider (RHIC) and CERN Large Hadron Collider (LHO), the multiplicity per participant will be larger. The effect of a change in the bombarding energy will be studied in Sec. V D. We recall that the multiplicity per unit rapidity and the transverse energy per unit rapidity are both proportional, to a good approximation, to the number of participants. In the following sections, we shall consider any of these quantities as a measure of the impact parameter.

D. Spatial anisotropy

The initial repartition of the entropy density is clearly anisotropic in the transverse plane for a peripheral collision, as can be seen in Fig. 1. As we explained in Sec. II B, this anisotropy initially present in the spatial distributions is at the origin of the anisotropy in momentum distributions. It is therefore interesting to define a measure of this spatial anisotropy. For this purpose, consider the region in the (x,y) plane where the initial entropy density is at least equal to half its maximum value. If L_x is the size of this region in the x direction (direction of impact parameter) and L_y its size in the orthogonal direction y ($L_y > L_x$), a natural measure of the spatial anisotropy α_s is

$$\alpha_s \equiv \frac{L_y - L_x}{L_y + L_x} . \tag{4.18}$$

α_s can then be computed as a function of impact parameter for a given colliding system, or equivalently, as a function of the number of participating nucleons. The result is displayed in Fig. 3. As expected, α_s is an increasing function of impact parameter and thus a decreasing function of the number of participants N, and it vanishes for central collisions as a consequence of isotropy. The decrease of α_s for very peripheral collisions is an effect of the skin thickness of the nuclei, ξ, which enters the parametrization of the nuclear density in Eq. (4.16). Since ξ is approximately the same for all nuclei, this effect is more important for smaller nuclei such as S, where ξ is larger compared to the size of the nucleus than for a heavy nucleus. Note that the decrease of α_s with N is approximately linear for the three colliding systems considered here. The maximum value of α_s is about 0.3 for a Pb-Pb collision, and somewhat smaller for the two other systems. Thus, α_s tends to increase with size of target and/or projectile.

We expect that the anisotropy in transverse momenta,

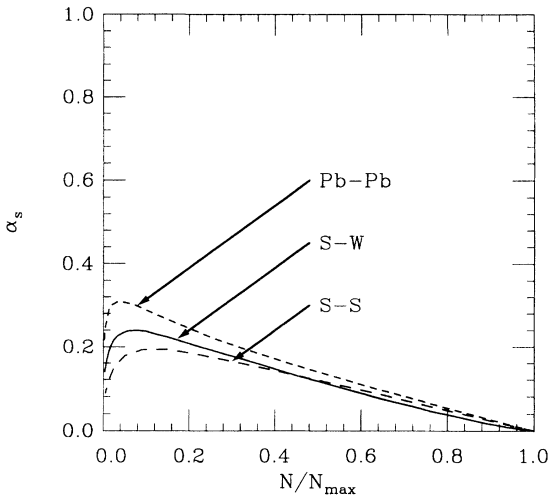

FIG. 3. Spatial anisotropy for various colliding systems. α_s, defined by Eq. (4.18), is plotted against the number of participating nucleons, scaled to its maximum value (reached for a central collision) N_{max}. Short dashes: lead-lead collision ($N_{max} \simeq 395$). Long dashes: sulfur-sulfur collision ($N_{max} \simeq 51$). Solid line: sulfur-tungsten collision ($N_{max} \simeq 121$).

$\bar{\alpha}$, will be comparable to the spatial anisotropy α_s. However, while α_s only involves the initial conditions, other parameters come into play in the determination of $\bar{\alpha}$, which are the parameters of hydrodynamics: initial time, decoupling temperature, and equation of state. In Secs. V and VI, we study their influence on $\bar{\alpha}$.

V. MASSLESS PION GAS

The simplest equation of state one can think of is that of blackbody radiation, which corresponds here to taking only pions into account, and neglect their mass and interactions. The entropy density s is then

$$s(T) = \frac{2\pi^2}{45} \nu_h T^3 , \tag{5.1}$$

where $\nu_h = 3$ is the pion degeneracy factor. Such an equation of state considerably overestimates the temperature for a given density, as is shown [12,14] by a discussion of the average transverse momentum $\langle p_T \rangle$. However, we use it as a reference case because it does not contain any dimensional parameter: thus, the only temperature scale in the problem is the initial temperature.

A. Variation of $\bar{\alpha}$ with the multiplicity

Using Eq. (5.1), we computed the anisotropy $\bar{\alpha}$ defined by Eq. (4.9) as a function of the number of participants. We take the values $t_0 = 1$ fm/c for the initial time and $T_d = 150$ MeV/c for the decoupling temperature and postpone the discussion concerning these parameters until the following sections. The result is displayed in Fig. 4 for a Pb-Pb collision. $\bar{\alpha}$ is very close to the spatial anisotropy α_s displayed in Fig. 3, which shows that the anisotropy in the final momenta is tightly related to the spatial

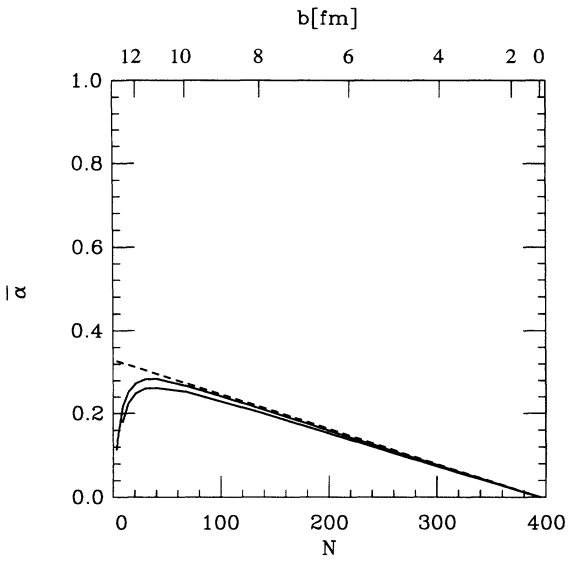

FIG. 4. Lead-lead collision and equation of state of a massless pion gas. Solid lines: anisotropy $\bar{\alpha}$ as a function of the number of participating nucleons N. The impact parameter b is also shown on the horizontal scale. The decoupling temperature is $T_d = 150$ MeV. The initial time is $t_0 = 2$ fm/c for the lower curve and $t_0 = 1$ fm/c for the upper curve. Dashed line: linear approximation, Eq. (5.2).

anisotropy in the initial conditions. The only difference is for very peripheral collisions with $b > 12$ fm where the decrease of $\bar{\alpha}$ is more important than that of α_s. We shall comment on this later in this section. The variation of $\bar{\alpha}$ with N is almost linear, so that the formula

$$\bar{\alpha} = \alpha_{\max}(1 - N/N_{\max}) \tag{5.2}$$

with $\alpha_{\max} = 0.33$ and $N_{\max} \simeq 395$ (value of N for a central collision) reproduces the numerical results remarkably well down to $N = N_{\max}/10$.

B. Influence of the initial time

The initial time t_0 fixes the beginning of hydrodynamical expansion. One expects this time to be of the order of 1 fm/c, which is the order of magnitude of the time it takes the nuclei to cross each other, and also the typical scale for the formation of particles. However, it is difficult to estimate this time accurately. Even the concept of initial time is itself a simplification: since the initial density is not homogeneous, different parts of the system can thermalize at different times. Thus, it is necessary to study how a modification of t_0 affects the anisotropy.

In fact, it is easy to show [10] that the transverse collective flow is not much affected by a change of the thermalization time t_0 as long as the latter remains much smaller than the transverse size R_0 of the system, which is as large as 7 fm/c for a central lead-lead collision. The argument is the following: at a small time τ after thermalization, the fluid velocity is proportional to τ according to the relativistic Euler equation

$$|\mathbf{v}| = \left| -\frac{\nabla P}{w}\tau \right| \sim \frac{\tau}{R_0} , \tag{5.3}$$

where $w = 4P$ is the enthalpy density and R_0 is a typical transverse size. Thus, the transverse velocity is, in any case, small at times much smaller than R_0. Therefore, if one changes the thermalization time from $t_0 \ll R_0$ to $t_0' \ll R_0$, one expects that any observable associated with transverse collective flow (and, in particular, the anisotropy $\bar{\alpha}$) undergoes a relative change of order $(t_0' - t_0)/R_0 \ll 1$, which can be neglected in a first approximation. The hypothesis that $t_0 \ll R_0$ thus allows one to get rid of the uncertainty on t_0. However, it is not satisfied for very peripheral collisions where the transverse dimensions are smaller, and where the thermalization time could also be bigger since the density is lower.

The results of numerical calculations carried out with two different values of t_0 are displayed in Fig. 4. As expected, the difference between the two curves is negligible except for small multiplicities, which correspond to very peripheral collisions where $t_0 \sim R_0$.

C. Influence of the decoupling temperature

While t_0 fixes the time when hydrodynamic expansion starts, the decoupling temperature tells us when it stops. One usually assumes that T_d is of the order of the pion mass, but its precise value remains uncertain. The smaller T_d, the longer hydrodynamics lasts. Since collective flow creates anisotropy, one naturally expects $\bar{\alpha}$ to increase with decreasing T_d: if T_d is as big as the initial temperature T_0, the system decouples as soon as it thermalizes and since the initial distribution is isotropic in the transverse plane, $\bar{\alpha}$ is zero; in the limit $T_d \to 0$, on the other hand, $\bar{\alpha}$ reaches its maximum value. (This is, in fact, not always true, but we shall come back to this point in Sec. VI A.) The question which arises is whether there is a typical scale for T_d, under which the variations of $\bar{\alpha}$ can be neglected. In fact, once the transverse expansion has fully developed, one intuitively expects $\bar{\alpha}$ to increase only slowly with time. The time it takes for the transverse expansion to develop is of the order of the transverse size R_0 of the system. The typical temperature at this time, which we refer to as the effective temperature T_{eff}, can be estimated simply: since longitudinal expansion dominates for $t_0 < R_0$, the entropy density decreases like [6] $1/t$. Using Eq. (5.1), the temperature at $t = R_0$ is then approximately given by

$$T_{\text{eff}} \simeq T_0 (t_0/R_0)^{1/3} \tag{5.4}$$

and one expects the anisotropy to vary slowly with T_d if $T_d < T_{\text{eff}}$.

Concerning the impact-parameter dependence, two effects must be considered: First, T_d (which is the temperature at which the mean free path equals the dimension of the system) is larger for a smaller system, and thus in-

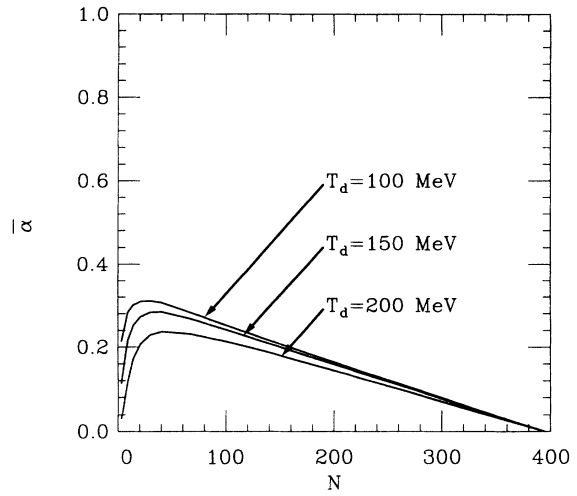

FIG. 5. Same as Fig. 4 with three different values of the decoupling temperature T_d.

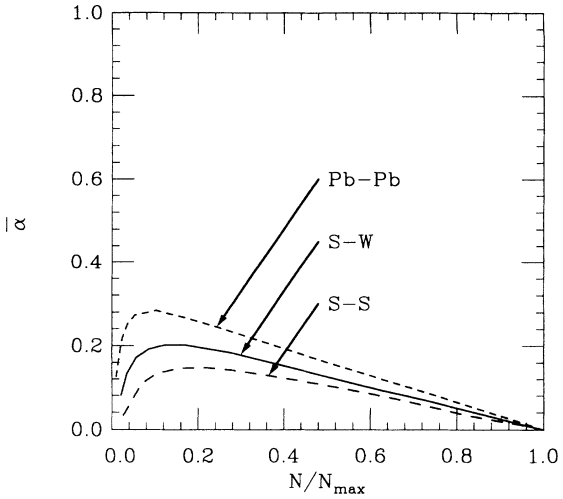

FIG. 6. Comparison between various colliding systems. $\bar{\alpha}$ is plotted against the number of participating nucleons scaled to its maximum value N_{max}, as in Fig. 4. The decoupling temperature is $T_d = 150$ MeV and the initial time $t_0 = \text{fm}/c$ for the three curves.

creases with impact parameter. However, this variation is small [10] and we neglect it. The second effect is that for peripheral collisions the system is colder and smaller. It thus has a smaller effective temperature T_{eff}. When T_{eff} becomes as low as the decoupling temperature T_d, the variation of $\bar{\alpha}$ with T_d is strong: the system freezes before transverse expansion has time to develop. This effect accounts for the observed decrease of $\bar{\alpha}$ for very peripheral collisions. In other terms, we expect that increasing T_d has qualitatively the same effect as increasing t_0: it affects mostly peripheral collision with a transverse size $R_0 \sim t_0$ in the latter case or $T_d \simeq T_{\text{eff}}$ in the former.

Numerical results are displayed in Fig. 5 for a lead-lead collision. The effective temperature is of the order of 275 MeV for a central collision with this equation of state; i.e., it is much higher than the decoupling temperatures. As expected, the influence of T_d on $\bar{\alpha}$ is rather weak except for very peripheral collisions which have smaller effective temperatures. The results we have obtained so far show that, although t_0 and T_d are to some extent free parameters, they do not influence the anisotropy much.

D. Other colliding systems

First, let us discuss the effect of changing the bombarding energy. This has *a priori* two effects. First, the inelastic nucleon-nucleon cross section σ_{in} used to calculate the number of participants in Eq. (4.17) varies with the beam energy. However, this dependence is weak, and it has little influence on the number of participants. Second, the multiplicity per participant increases with the beam energy. As a consequence, the initial entropy density is multiplied by an overall factor, and so is the initial temperature T_0. Now, there is no temperature scale in the equation of state Eq. (5.1); thus, the only temperatures in the problem are the initial temperature T_0 and the decoupling temperature T_d. The anisotropy $\bar{\alpha}$, which is a dimensionless quantity, can depend only on T_d/T_0. Thus, a change in the initial temperature amounts to a change in the decoupling temperature, which has minor effects as discussed in Sec. V C. Hence, the results of this section are, to a good approximation, independent of the bombarding energy.

Now, we would like to discuss how $\bar{\alpha}$ is sensitive to the size of the nuclei. First, note that the equations of hydrodynamics are scale invariant. Therefore, a change of scale in the initial conditions merely results in a change of scale (space and time) in the flow, which does not change the value of α. Then there are only two ways α can depend on the size of the nuclei. The first way is through t_0 or T_d, whose dependence on the size may be nontrivial, but these are small effects, as we showed earlier in Secs. V B and V C. The second way is through the shape of the initial density profile. We know from Sec. IV D that this shape induces a dependence of the spatial anisotropy α_s on the target and projectile sizes. We therefore expect the same qualitative dependence for the anisotropy in momenta, $\bar{\alpha}$. Numerical results are displayed in Fig. 6, where this prediction can be verified: the curves are similar to those in Fig. 3, and $\bar{\alpha}$, like the spatial anisotropy α_s, increases with size of target and/or projectile. However, the dependence is somewhat stronger for $\bar{\alpha}$, which is smaller by a factor of almost 2 in a S-S collision than in a Pb-Pb collision.

Finally, let us mention that we have only discussed spherical nuclei, for simplicity. But if the collision involves one or two deformed nuclei such as ^{238}U, some anisotropy is present even for very central collisions. For a given multiplicity, the values of $\bar{\alpha}$ will be spread over a whole interval according to the orientations of the nuclei relative to the collision axis and relative to each other.

VI. OTHER EQUATIONS OF STATE

As we already mentioned in the Introduction, the equation of state is a crucial ingredient in hydrodynam-

ics. In this section, we study its influence on $\bar{\alpha}$. However, we proceed indirectly. First, we recall the conditions under which a scaling solution develops in the hydrodynamic expansion. This will provide us with a deeper understanding of how initial conditions affect the hydrodynamic flow, and hence how anisotropy appears, since we have shown that the anisotropy in momentum distributions originates from the initial spatial anisotropy.

A. Scaling solutions in hydrodynamics

The study of scaling solutions in relativistic hydrodynamics was pioneered by Landau [8]. Here we define a scaling solution as a flow where the fluid velocity satisfies $\mathbf{v}=\mathbf{x}/t$: the expansion is homogeneous and isotropic, much like the expansion of the Universe. Landau showed that for a one-dimensional expansion a scaling solution always develops at long times. His study was generalized later by Cooper, Frye, and Schonberg in three dimensions [16]. They find that a scaling solution may appear in three dimensions only if the equation of state satisfies $c_s^2<\frac{1}{5}$. This result can be easily generalized to an arbitrary number of dimensions D where this condition becomes

$$(2D-1)c_s^2<1 \ . \tag{6.1}$$

This is a necessary condition for the scaling solution to exist, but it is not clear whether it is sufficient, i.e., whether a scaling solution is always reached asymptotically when condition (6.1) is satisfied. However, we retain the qualitative idea that a scaling solution is favored by a smaller number of dimensions D and a smaller speed of sound.

Why is this discussion relevant to our study? We are dealing with a three-dimensional expansion: in our model, the longitudinal expansion satisfies the scaling relation $v_z=z/t$ by construction according to Bjorken's scenario, but the transverse velocity can satisfy the scaling relation only asymptotically since it is initially zero. Now, the scaling solution is isotropic. As such, it does not keep the memory of the initial conditions which are not necessarily isotropic. Thus, $\bar{\alpha}$ is zero if a scaling solution develops, and we expect that the effects which favor the apparition of a scaling solution (lower number of dimensions or lower velocity of sound) tend to decrease the anisotropy. We calculated numerically $\bar{\alpha}$ as a function of the decoupling temperature T_d with a very low value of the speed of sound, $c_s^2=\frac{1}{10}$, which satisfies Eq. (6.1) in three dimensions. We checked that when T_d decreases (i.e., when the time of hydrodynamical expansion increases), $\bar{\alpha}$ first increases (remember that $\bar{\alpha}=0$ if T_d is greater than the initial temperature), passes through a maximum, and then decreases, as expected if a scaling solution develops. However, this decrease is very slow and it is therefore hard to check whether $\bar{\alpha}\to 0$ for vanishing T_d (i.e., for infinite time).

B. Effect of the longitudinal expansion

It might be thought naively that longitudinal expansion has hardly any effect on the anisotropy since anisotropy comes from the transverse collective expansion. However, the previous argument shows that lowering the dimension D favors the apparition of a scaling solution, and thus $\bar{\alpha}$ should be smaller without the longitudinal expansion ($D=2$) than with Bjorken scenario ($D=3$). We performed two series of calculations: one with regular longitudinal expansion, according to Bjorken's scenario, and one with no longitudinal expansion. Numerical results are shown in Fig. 7 where one sees that the qualitative effect is correct: although $\bar{\alpha}$ still remains quite large in the two-dimensional case, it is smaller by about 15% than in the three-dimensional case.

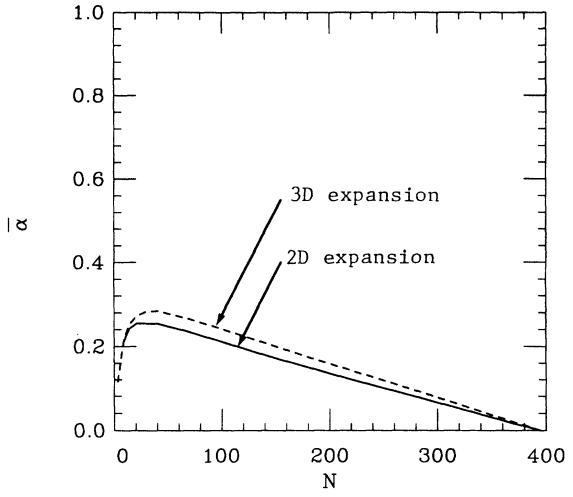

FIG. 7. Effect of the longitudinal expansion. Dashed line: same as the solid line in Fig. 4 (regular longitudinal expansion, scaling regime). Solid line: no longitudinal expansion.

This result is interesting not only because it confirms the relation between scaling solutions and anisotropy, but also in itself: indeed, it is not clear whether Bjorken's scenario gives a reliable description of current experiments, where nuclear stopping is still large. Thus, it is interesting to consider the influence of the longitudinal expansion. Bjorken's scaling solution $v_z=z/t$ corresponds to the fastest possible longitudinal expansion; Landau's model, which assumes that the initial fluid velocity is initially zero everywhere, would give a slower longitudinal expansion even if a scaling solution eventually develops. Therefore, assuming no longitudinal expansion at all gives a value of $\bar{\alpha}$ which is at most 15% lower than with the maximum longitudinal expansion.

C. Varying the speed of sound

Here, we want to study how $\bar{\alpha}$ depends on the speed of sound c_s, which plays a crucial role in all hydrodynamic phenomena. For this purpose, we consider a parametrization of the hadronic equation of state proposed by Shuryak [17]:

$$s(T)=\frac{6}{5}\frac{T^5}{T_1^4}, \quad T_1=100 \text{ MeV} \ . \tag{6.2}$$

The speed of sound in Eq. (6.2) is constant, its value being $c_s^2=d(\ln T)/d(\ln s)=\frac{1}{5}$, which is smaller than the ideal massless gas value $c_s^2=\frac{1}{3}$. This equation of state is probably closer to reality than Eq. (5.1), although it is still a crude approximation.

Note that, unlike Eq. (5.1), Eq. (6.2) involves a temperature scale T_1. However, we are going to show that the anisotropy cannot depend much on T_1. First, note that the equations of hydrodynamics do not involve the temperature but only the energy density ϵ and the pressure P. Now, the relation between ϵ and P is $P=\epsilon/5$ since the speed of sound is constant, and it does not involve T_1. Thus, the only temperatures in the problem are the initial temperature T_0 and the decoupling temperature T_d, as in Sec. V, and $\bar{\alpha}$ may only depend on the dimensionless ratio T_d/T_0. However, T_0 depends on T_1. Indeed, what is given initially is the entropy density, which we calculate independently of the equation of state (Sec. IV C). Then, according to Eq. (6.2), the initial temperature T_0 is proportional to $T_1^{2/5}$ for a given entropy density. Thus, the only effect of changing T_1 is a scaling of the temperature of the system proportionally to $T_1^{2/5}$. If we express the anisotropy $\bar{\alpha}$ as a function of T_1 and the decoupling temperature T_d, all other quantities being held fixed, then

$$\bar{\alpha}(\lambda T_1, T_d)=\bar{\alpha}(T_1, \lambda^{-2/5} T_d) \ . \tag{6.3}$$

This means that a change in T_1 amounts to a change in the decoupling temperature, which has minor effects on $\bar{\alpha}$ as we discussed in Sec. V C.

According to Eq. (6.1) and the discussion of Sec. VI A, we expect that lowering the speed of sound c_s has the same effect as lowering the number of dimensions D. That is, we expect $\bar{\alpha}$ to decrease with decreasing c_s. Numerical results with $c_s^2=\frac{1}{3}$ and $c_s^2=\frac{1}{5}$ are displayed in Fig. 8. Since we did not want to express Eq. (6.2) explicitly in terms of particles, we only calculated the upper and lower bounds on $\bar{\alpha}$ derived in Sec. IV B. One sees that the predicted behavior is correct; i.e., $\bar{\alpha}$ is somewhat smaller with a smaller speed of sound.

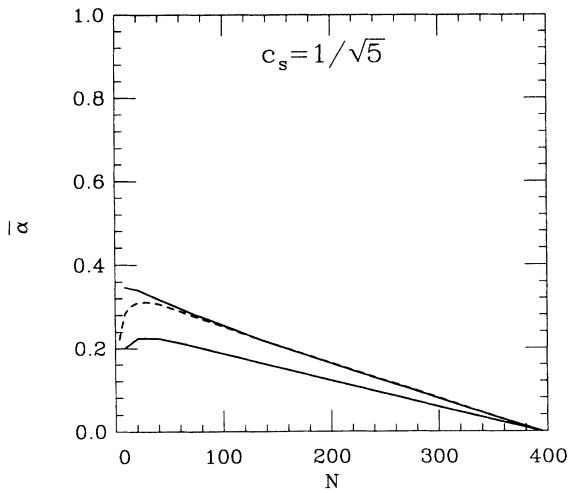

FIG. 8. Results of the calculation carried out with Eq. (6.2) for a lead-lead collision, with $t_0=1$ fm/c and $T_d=100$ MeV. The two solid lines give the upper and lower bound on $\bar{\alpha}$, calculated from Eq. (4.10) with $C(T_d)=0$ (upper curve) and $C(T_d)=A(T_d)/3$ (lower curve), which correspond to the bounds on C in Eq. (4.8). The dashed line shows, for sake of comparison, the value of $\bar{\alpha}$ for a massless pion gas, as in Fig. 5.

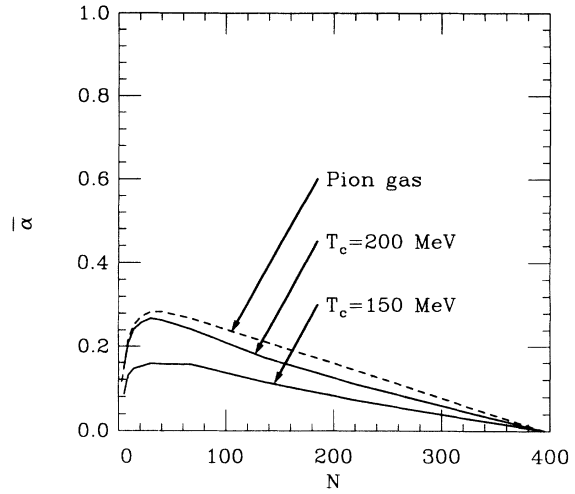

FIG. 9. Effect of quark-gluon-plasma formation. Dashed line: same as Fig. 4 (no phase transition). Solid line: first-order phase transition at $T=T_c$.

D. Effect of quark-gluon-plasma formation

In order to study the influence of a phase transition coming from the possible formation of a quark-gluon plasma, we use a bag-model equation of state for the high-temperature phase, keeping Eq. (5.1) for the low-temperature phase:

$$s(T)=\frac{2\pi^2}{45}T^3\{\nu_h[1-\theta(T-T_c)]+\nu_{\rm pl}\theta(T-T_c)\} \ , \tag{6.4}$$

where T_c is the critical temperature and $\nu_{\rm pl}=37$ is the number of effective degrees of freedom for a massless quark-gluon plasma with two flavors.

It is well known that a phase transition slows down the transverse expansion [18], and thus we expect $\bar{\alpha}$ to be smaller if the system undergoes a phase transition. This effect can be seen clearly in Fig. 9. It is stronger for the lower critical temperature, where a longer time is spent in the high-temperature phase.

Let us summarize the results obtained in this section: the anisotropy is favored by a strong longitudinal expansion, as in Bjorken's scenario, or by a high value of the velocity of sound c_s. However, suppressing the longitudinal expansion or lowering c_s implies a decrease of $\bar{\alpha}$ which does not exceed 25%. On the other hand, a strong first-order phase transition from a quark-gluon plasma may reduce $\bar{\alpha}$ by a factor of 2 if the critical temperature is of the order of 150 MeV.

VII. DISCUSSION

Now we come back to the finite multiplicity fluctuations discussed in Sec. III in order to discuss under which conditions they may mask the anisotropy coming

from collective effects. Our goal is to define the optimal experimental conditions to detect collective effects. Equation (3.15) gives a general form of the condition under which the anisotropy $\bar{\alpha}$ in the emission probability can be seen as a maximum in the probability distribution of the observed α. Let us now see what this condition becomes in the frame of a hydrodynamical model.

First of all, δ depends on the shape of the momentum distribution. The determination of δ must eventually come from the experiment itself, but it is, however, instructive to evaluate it in a hydrodynamical model. We show in Appendix B that, for a fluid composed of massless bosons, δ is always comprised between 3.38 and 4.06. Thus, it is higher than with a Gaussian ($\delta=2$) or even with an exponential ($\delta=\frac{10}{3}$) p_T distribution. If the particles are massive, then δ is smaller provided that the chemical potential is zero. Thus, we may write in any case $\delta<4.06$. Note, however, that hard processes enhance significantly the high-p_T tail and might therefore produce a higher value of δ.

Now, for a given experiment (given nuclei, given bombarding energy), we have shown that the anisotropy expected on the basis of a hydrodynamical model varies linearly with the number of participants according to Eq. (5.2), except for very peripheral collisions. Since the observed multiplicity is, to a good approximation, proportional to the number of participants, we may write Eq. (5.2) in the form

$$\bar{\alpha}=\alpha_{\max}\left[1-\frac{M}{M_{\max}}\right], \tag{7.1}$$

where $\bar{\alpha}$ is the anisotropy from hydrodynamics for an observed multiplicity M, $M_{\max}$ is the observed multiplicity for a central collision, and $\alpha_{\max}$ depends mainly on the equation of state and the nuclei involved in the collision. Note that the observed multiplicity M depends on the detector used in the experiment (efficiency, coverage in rapidity, type of particles measured, etc.). Comparing with Eq. (3.15), one finds that the condition for the anisotropy to be detected at a given multiplicity M can be written

$$\left[\frac{M}{M_{\max}}\right]^{1/2}\left[1-\frac{M}{M_{\max}}\right]>\left[\frac{\delta}{M_{\max}\alpha_{\max}^2}\right]^{1/2}. \tag{7.2}$$

This condition is depicted graphically in Fig. 10. It is satisfied neither for central collisions (M close to $M_{\max}$) where the anisotropy is too small, nor for very peripheral collisions ($M \ll M_{\max}$) where finite multiplicity fluctuations are too high. In fact, the optimal multiplicity $M_{\opt}$ to detect the anisotropy is obtained by maximizing the left-hand side of Eq. (7.2), which yields

$$M_{\opt}=\frac{M_{\max}}{3}. \tag{7.3}$$

Inserting this value into Eq. (7.2), one obtains the criterion for anisotropy to be detected at $M=M_{\opt}$:

$$M_{\max}>\frac{27\delta}{4}\frac{1}{\alpha_{\max}^2}. \tag{7.4}$$

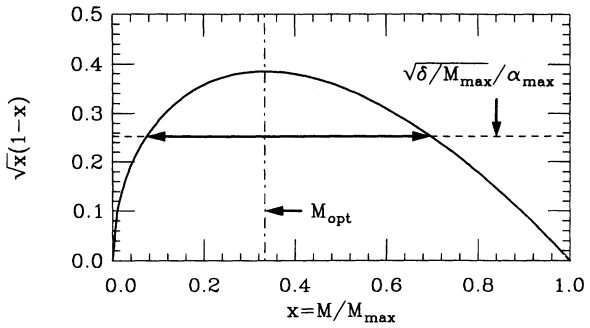

FIG. 10. Solid line: left-hand side of Eq. (7.2). Dashed line: right-hand side of the same equation for $\alpha_{\max}=0.25$, $M_{\max}=500$, $\delta=2$. Dash-dotted line: optimal value of the multiplicity $M_{\opt}$, defined by Eq. (7.3). The arrows indicate the interval of M over which Eq. (7.2) is satisfied, i.e., anisotropy can be seen experimentally.

Choosing $\delta=2$ as in Eq. (3.14) and the value $\alpha_{\max}\simeq 0.25$ obtained for a lead-lead collision and a physically reasonable speed of sound $c_s=1/\sqrt{5}$, the criterion Eq. (7.4) becomes $M_{\max}>216$. If δ is larger, the required $M_{\max}$ should be enlarged by the same factor. By measuring all charged particles within one rapidity unit in a central lead-lead collision at 160 GeV per nucleon in the laboratory frame [energy reached at the CERN Super Proton Synchrotron (SPS)], one expects $M_{\max}\simeq 600$ so that the anisotropy should be seen easily if present. On the other hand, for a sulfur-sulfur collision, we have seen in Sec. V D that $\alpha_{\max}$ is smaller by a factor of 2, so that the lower bound on the multiplicity is four times larger than for a lead-lead collision according to Eq. (7.4). But since the multiplicity scales approximately like the number of participants, it is about eight times lower for a central sulfur-sulfur than for a central lead-lead collision. Thus, it is very unlikely that collective effects can be seen in collisions involving light nuclei.

Figure 11 displays a comparison between corrected probability distributions $dP_{\text{cor}}/d\alpha$ calculated with an isotropic emission law (dashed curve) or with the value of anisotropy given by hydrodynamics (solid curves). We assume that the detector is such that $M_{\max}=500$ particle momenta are measured in a central collision. Finite multiplicity effects are calculated using a Gaussian parametrization as in Sec. III B. For the three first curves (a), (b), and (c), M lies within the interval defined in Fig. 10, where collective effects result in a peak of the corrected probability at $\alpha\neq 0$, which is clearly seen in the figure. On the other hand, curve (d) corresponds to a more central collision. $\bar{\alpha}$ is too low and collective effects do not change much the probability distribution of α. Note that we have used a Gaussian parametrization of the momentum distribution, and the "isotropic" distributions (dashed curves) could be broader if a more realistic parametrization were considered.

To conclude, let us mention that we have only considered the fluctuations coming from uncorrelated momenta. However, one knows that correlations are present

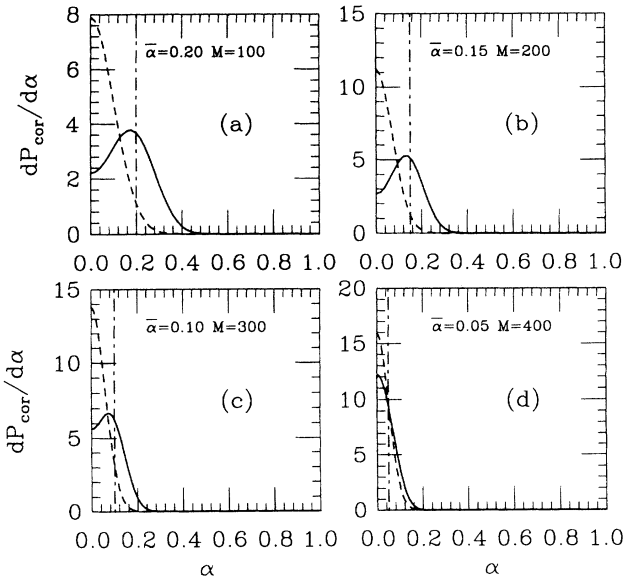

FIG. 11. Predictions for the probability distribution of α in a lead-lead collision, with various values of the impact parameter. We assume that the detector is such that $M_{max}=500$ particles are measured in a central collision. Then, to each value of the impact parameter corresponds a multiplicity M. We assume that the transverse-momentum distribution is Gaussian. The solid lines give the corrected probability when collective effects are present, calculated according to Eq. (3.13) with $\bar{\alpha}$ given by Eq. (7.1) (we take $\alpha_{max}=0.25$ as in Fig. 10). Dash-dotted lines indicate the value $\alpha=\bar{\alpha}$. The dashed lines give the corrected probability when there are no collective effects, calculated according to Eq. (3.10).

which are of various physical origin. Bose-Einstein correlations first, which always exist between identical particles, should be taken into account. Jet production also implies the emission of several particles with their momenta preferentially aligned along the jet direction. This could be a strong effect, possibly masking the anisotropy coming from hydrodynamical behavior. A more sophisticated treatment should include all these effects. However, anisotropy seems to be a rather promising signature of collective effects in ultrarelativistic heavy-ion reactions. It could be measured experimentally, and also in event generators including rescattering, and compared to the predictions of hydrodynamics.

ACKNOWLEDGMENTS

I wish to express my warmest thanks to Jean-Paul Blaizot for numerous discussions and fruitful comments on the manuscript. Service de Physique Théorique is Laboratoire de la Direction des Sciences de la Matière du Commissariat à l'Énergie Atomique.

APPENDIX A: FLUCTUATIONS WITH AN ARBITRARY UNCORRELATED DISTRIBUTION

Let us assume that the particles are emitted according to an uncorrelated distribution. Then the central limit theorem ensures that, for a large number of particles M, the probability law of the sphericity tensor (2.7) is Gaussian. $S_{ij}^{\perp}$ has three independent parameters which we rearrange in a vector S_i $(i=1,2,3)$ by defining

$$\begin{aligned} S_1 &= S_{11}^{\perp}+S_{22}^{\perp}=\sum_{\nu=1}^{M}(p_x^2+p_y^2)=\mathcal{E}\ , \\ S_2 &= S_{11}^{\perp}-S_{22}^{\perp}=\sum_{\nu=1}^{M}(p_x^2-p_y^2)=\mathcal{E}\alpha\cos 2\theta\ , \\ S_3 &= 2S_{12}^{\perp}=2\sum_{\nu=1}^{M}p_x p_y=\mathcal{E}\alpha\sin 2\theta\ , \end{aligned} \tag{A1}$$

where we have used the parametrization introduced in Eq. (3.1). Then the most general Gaussian distribution for S is of the form

$$\frac{dP}{dS_1\,dS_2\,dS_3}\propto\exp[-({}^tS-{}^t\bar{S})T^{-1}(S-\bar{S})/2]\ , \tag{A2}$$

where $\bar{S}=\langle S\rangle$ is the average value of S and T is the 3×3 covariance matrix defined by

$$T_{ij}=\langle S_iS_j\rangle-\bar{S}_i\bar{S}_j\ . \tag{A3}$$

Since the emission is uncorrelated, T_{ij} is proportional to the number of particles, M. The coordinate axes can always be chosen in such a way that $\langle p_xp_y\rangle=0$ and $\langle p_x^2\rangle>\langle p_y^2\rangle$ (for spherical nuclei, x is the direction of impact parameter). Then $\bar{S}$ can be expressed as

$$\begin{aligned} \bar{S}_1 &= \bar{\mathcal{E}}\ , \\ \bar{S}_2 &= \bar{\mathcal{E}}\bar{\alpha}\ , \\ \bar{S}_3 &= 0\ , \end{aligned} \tag{A4}$$

where $\bar{\mathcal{E}}=M\langle p_T^2\rangle$, and $\bar{\alpha}=(\langle p_x^2\rangle-\langle p_y^2\rangle)/(\langle p_x^2\rangle+\langle p_y^2\rangle)$ clearly represents the anisotropy in the emission probability. Let us now define dimensionless, scaled quantities Σ, $\bar{\Sigma}$, and Θ by $S=\mathcal{E}\Sigma$, $\bar{S}=\bar{\mathcal{E}}\bar{\Sigma}$, and $T=M^{-1}\bar{\mathcal{E}}^2\Theta$. Σ depends only on α and θ; as to Θ, it is independent of M since both T and $\bar{\mathcal{E}}$ are proportional to M. Using Eq. (3.2), one can rewrite Eq. (A2) as

$$\frac{dP}{d\alpha\,d\theta\,d\mathcal{E}}\propto\alpha\mathcal{E}^2\exp\left[-\frac{M}{2}\left[\frac{\mathcal{E}}{\bar{\mathcal{E}}}{}^t\Sigma-{}^t\bar{\Sigma}\right]\times\Theta^{-1}\left[\frac{\mathcal{E}}{\bar{\mathcal{E}}}\Sigma-\bar{\Sigma}\right]\right]\ . \tag{A5}$$

For large M, the exponential is strongly peaked at $\mathcal{E}=\bar{\mathcal{E}}({}^t\bar{\Sigma}\Theta^{-1}\Sigma)/({}^t\Sigma\Theta^{-1}\Sigma)$. Therefore, the factor $\mathcal{E}^2$ in front of the exponential can be dropped, and the integral over $\mathcal{E}$ is Gaussian:

$$\frac{dP}{d\alpha\,d\theta}\propto\frac{\alpha}{\sqrt{{}^t\Sigma\Theta^{-1}\Sigma}}\exp\left[\frac{M}{2}\frac{({}^t\bar{\Sigma}\Theta^{-1}\Sigma)^2}{{}^t\Sigma\Theta^{-1}\Sigma}\right]\ . \tag{A6}$$

The exponent in Eq. (A6) is maximal for $\Sigma=\bar{\Sigma}$. Therefore, the probability distribution is peaked at $\Sigma=\bar{\Sigma}$ and we may write $\Sigma=\bar{\Sigma}+\Lambda$, where Λ is a small quantity. Expanding the exponent in Eq. (A6) to second order in Λ, one gets

$$\frac{dP}{d\alpha\, d\theta} \propto \alpha \exp\left[\frac{M}{2}\frac{({}^t\bar{\Sigma}\Theta^{-1}\Lambda)^2-({}^t\bar{\Sigma}\Theta^{-1}\bar{\Sigma})({}^t\Lambda\Theta^{-1}\Lambda)}{{}^t\bar{\Sigma}\Theta^{-1}\bar{\Sigma}}\right] . \tag{A7}$$

We have dropped the factor $1/\sqrt{{}^t\Sigma\Theta^{-1}\Sigma}$ in front of the exponential since $\Sigma\simeq\bar{\Sigma}$. Note that, since Θ^{-1} is a positive symmetric matrix, the numerator in Eq. (A7) is negative for $\Lambda\neq 0$, which proves that the exponential is indeed maximal for $\Lambda=0$. Equation (A7) is quite general. Its right-hand side depends on α and θ through $\Lambda=(0,\alpha\cos 2\theta-\bar{\alpha},\alpha\sin 2\theta)$, and it must be integrated over the angle θ in order to get the probability distribution for α. Before doing this, we make a few simplifications. For spherical nuclei, we know that the colliding system is symmetric with respect to the reaction plane. We therefore expect the emission probability to be symmetric under $p_y\rightarrow -p_y$. This implies

$$\Theta_{13}=\langle S_1 S_3\rangle/M\langle p_T^2\rangle^2=2\langle p_x^3 p_y+p_x p_y^3\rangle/\langle p_T^2\rangle^2=0$$

and similarly, $\Theta_{23}=0$. After some algebra, Eq. (A7) then becomes

$$\frac{dP}{d\alpha\, d\theta} \propto \alpha \exp\left\{-\frac{M}{2}\left[\frac{(\alpha\cos 2\theta-\bar{\alpha})^2}{\Theta_{22}-2\Theta_{12}\bar{\alpha}+\Theta_{11}\bar{\alpha}^2}+\frac{(\alpha\sin 2\theta)^2}{\Theta_{33}}\right]\right\} . \tag{A8}$$

In order to integrate this expression over θ, approximations must be made.

First, consider the case when $\bar{\alpha}\ll 1$. Then we assume that the covariance matrix T has approximately the same form as for an isotropic distribution. Note that this is not true, in general, since even an anisotropic emission probability can give rise to $\bar{\alpha}=0$ (imagine, for instance, that the particle momenta are directed with probability $\frac{1}{2}$ along the x axis and with probability $\frac{1}{2}$ along the y axis). However, this is of little relevance to our problem since $\bar{\alpha}=0$ for central collisions only, and the emission probability is isotropic for central collisions. For an isotropic distribution, one easily verifies that T is diagonal using Eq. (A3). Introducing the dimensionless parameter

$$\delta=\langle p_T^4\rangle/\langle p_T^2\rangle^2 , \tag{A9}$$

the elements of the scaled covariance matrix Θ are given by

$$\Theta_{11}=\delta-1 ,$$
$$\Theta_{22}=\Theta_{33}=\delta/2 . \tag{A10}$$

Inserting these values in Eq. (A7) and keeping only terms of order α^2, one gets

$$\frac{dP}{d\alpha\, d\theta} \propto \alpha \exp\left[-\frac{M}{\delta}(\alpha^2-2\alpha\bar{\alpha}\cos 2\theta)\right] . \tag{A11}$$

If the emission probability is strictly isotropic ($\bar{\alpha}=0$), then $dP/d\alpha\, d\theta$ is independent of the angle θ as expected, and the probability distribution for α is simply

$$\frac{1}{\alpha}\frac{dP}{d\alpha} \propto \exp\left[-\frac{M\alpha^2}{\delta}\right] . \tag{A12}$$

This shows that the corrected probability distribution defined by Eq. (3.3) is always a Gaussian peaked at $\alpha=0$ if the emission probability is isotropic. It depends on the p_T distribution only through its width $\sqrt{\delta/2M}$, which involves the parameter δ defined by Eq. (A9). If $\bar{\alpha}\neq 0$ (but still $\bar{\alpha}\ll 1$), integration of Eq. (A11) over θ yields

$$\frac{1}{\alpha}\frac{dP}{d\alpha} \propto \exp\left[-\frac{M\alpha^2}{\delta}\right] I_0\left[\frac{2M\alpha\bar{\alpha}}{\delta}\right] , \tag{A13}$$

where I_0 is the modified Bessel function of order 0. With the Gaussian parametrization of the momentum distribution used in Sec. III B, we have checked numerically that Eq. (A13) with $\delta=2$ (which is the appropriate value for an isotropic Gaussian distribution) fits quite well the curves displayed in Fig. 2, which are obtained from the exact result Eq. (3.13). Finally, let us derive the condition under which the corrected distribution defined by Eq. (3.3) has a maximum at $\alpha\neq 0$. This is done most simply by expanding Eq. (A11) to order α^2 and then integrating over θ, which gives the condition

$$\bar{\alpha}>\sqrt{\delta/M} \tag{A14}$$

in agreement with Eq. (3.14) for a Gaussian momentum distribution. This means that the anisotropy in the emission law, $\bar{\alpha}$, results in a peak of the corrected probability distribution only if it is at least as the finite multiplicity fluctuations for α, which are of order $\sqrt{\delta/M}$ according to Eq. (A12). Note that if $\bar{\alpha}\gg\sqrt{\delta/M}$, the probability law of α, Eq. (A13), is simply a Gaussian peaked at $\alpha=\bar{\alpha}$:

$$\frac{1}{\alpha}\frac{dP}{d\alpha} \propto \exp\left[-\frac{M(\alpha-\bar{\alpha})^2}{\delta}\right] . \tag{A15}$$

Let us now study the case of a more strongly anisotropic distribution, where $\bar{\alpha}$ is of order unity. Since $M\gg 1$, this implies $\bar{\alpha}\gg 1/\sqrt{M}$, which means that anisotropy in the emission probability is much larger than statistical fluctuations. Then the integral over θ in Eq. (A7) can be done using the saddle-point method (the matrix elements of Θ are of order unity), which gives

$$\frac{1}{\alpha}\frac{dP}{d\alpha} \propto \exp\left[-\frac{M}{2}\frac{(\alpha-\bar{\alpha})^2}{\Theta_{22}-2\Theta_{12}\bar{\alpha}+\Theta_{11}\bar{\alpha}^2}\right] , \tag{A16}$$

which is a Gaussian centered at $\alpha=\bar{\alpha}$, as expected. Let us introduce three dimensionless parameters δ_1, δ_2, and δ_3:

$$\delta_1=\langle p_x^4\rangle/\langle p_x^2\rangle^2 ,$$
$$\delta_2=\langle p_y^4\rangle/\langle p_y^2\rangle^2 , \tag{A17}$$
$$\delta_3=\langle p_x^2 p_y^2\rangle/\langle p_x^2\rangle\langle p_y^2\rangle .$$

Then the matrix elements of Θ can be expressed as a function of $\bar{\alpha}$ and the δ_i, and Eq. (A16) becomes

$$\frac{1}{\alpha}\frac{dP}{d\alpha} \propto \exp\left[-\frac{2M}{\delta_1+\delta_2-2\delta_3}\left[\frac{\alpha-\bar{\alpha}}{1-\bar{\alpha}^2}\right]^2\right] . \quad \text{(A18)}$$

For a weakly anisotropic distribution ($\bar{\alpha} \ll 1$), $\delta_1 \simeq \delta_2 \simeq 3\delta/2$, $\delta_3 \simeq \delta/2$, and one recovers Eq. (A15). For the Gaussian parametrization considered in Sec. III B, $\delta_1=\delta_2=3$, $\delta_3=1$, and one recovers Eq. (3.12).

In summary, the results we have obtained allow to calculate the probability distribution of α in any case provided $M \gg 1$. If $\bar{\alpha} \ll 1$, Eq. (A13) gives the result, while Eq. (A18) must be used if $\bar{\alpha} \gg 1/\sqrt{M}$. If both conditions hold, that is, if $1/\sqrt{M} \ll \bar{\alpha} \ll 1$, both Eqs. (A18) and (A13) reduce to Eq. (A15).

APPENDIX B: MOMENTS OF THE MOMENTUM DISTRIBUTION

The moments of the momentum distribution Eq. (4.2) can be simply related to hydrodynamic quantities. Indeed, the first moment of the distribution is simply the particle number current:

$$\int p^\mu d\mu(p) = nu^\mu , \quad \text{(B1)}$$

where n is the particle number density measured in the rest frame of the fluid. The second moment is the familiar energy-momentum tensor

$$\int p^\mu p^\nu d\mu(p) = T^{\mu\nu} = wu^\mu u^\nu - Pg^{\mu\nu} , \quad \text{(B2)}$$

where P is the pressure, $w=\epsilon+P$ is the enthalpy density, and $g^{\mu\nu}=\mathrm{diag}(1,-1,-1,-1)$ is the metric tensor.

Let us now calculate the third-order moment of the distribution $S^{\mu\nu\rho}$ defined by Eq. (4.4). Since u^μ is the only four-vector at our disposal, Lorentz invariance ensures that $S^{\mu\nu\rho}$ is of the form

$$S^{\mu\nu\rho} = Au^\mu u^\nu u^\rho - C(g^{\mu\nu}u^\rho + g^{\nu\rho}u^\mu + g^{\rho\mu}u^\nu) , \quad \text{(B3)}$$

where A and C are Lorentz scalars. Now, contraction of any two indices in Eqs. (4.4) and (B3) yields immediately, using Eq. (B1),

$$S^{\mu\nu}{}_\nu = m^2 nu^\mu = (A-6C)u^\mu , \quad \text{(B4)}$$

which provides a relation between the two unknown coefficients A and C in Eq. (B3). Thus, only one coefficient of $S^{\mu\nu\rho}$ must be calculated in order to determine the whole tensor. It is clear from Eqs. (B1) and (4.4) that S^{000}/nu^0 is the average value of E^2 in the fluid, where E is the energy of a particle. In the rest frame of the fluid, this becomes, using Eq. (B3),

$$S^{000} = \langle\langle E^2 \rangle\rangle n = A - 3C , \quad \text{(B5)}$$

where the double angular brackets denote average values measured in the rest frame of the fluid. Thus, $\langle\langle E^2 \rangle\rangle$ can be expressed as a function of thermodynamic quantities only. Equations (B4) and (B5) give

$$\begin{aligned} A &= (2\langle\langle E^2 \rangle\rangle - m^2)n , \\ C &= \frac{\langle\langle E^2 \rangle\rangle - m^2}{3} n . \end{aligned} \quad \text{(B6)}$$

Higher-order moments can be calculated in a similar way. We now consider the fifth-order moments, which are required to calculate the parameter δ defined in Eq. (A9). We define

$$S^{\mu\nu\rho\sigma\tau} = \int p^\mu p^\nu p^\rho p^\sigma p^\tau d\mu(p) . \quad \text{(B7)}$$

Lorentz invariance allows one to write

$$\begin{aligned} S^{\mu\nu\rho\sigma\tau} = {} & A' u^\mu u^\nu u^\rho u^\sigma u^\tau \\ & - B'[u^\mu u^\nu u^\rho g^{\sigma\tau} + \text{permutations (10 terms)}] \\ & + C'[u^\mu g^{\nu\rho} g^{\sigma\tau} + \text{permutations (15 terms)}] . \end{aligned} \quad \text{(B8)}$$

Contracting over two indices in Eqs. (B7) and (B8) yields, using Eq. (4.4),

$$\begin{aligned} S^{\mu\nu\rho\sigma}{}_\sigma &= m^2 S^{\mu\nu\rho} \\ &= (A' - 10B')u^\mu u^\nu u^\rho \\ &\quad - (B' - 8C')(g^{\mu\nu}u^\rho + g^{\nu\rho}u^\mu + g^{\rho\mu}u^\nu) . \end{aligned} \quad \text{(B9)}$$

Using Eqs. (B3) and (B6), one gets two relations between A', B', and C':

$$\begin{aligned} A' - 10B' &= m^2(2\langle\langle E^2 \rangle\rangle - m^2)n , \\ B' - 8C' &= m^2(\langle\langle E^2 \rangle\rangle - m^2)n/3 . \end{aligned} \quad \text{(B10)}$$

A third equation is obtained by writing Eq. (B8) in the rest frame of the fluid:

$$A' - 10B' + 15C' = n\langle\langle E^4 \rangle\rangle . \quad \text{(B11)}$$

Equations (B10) and (B11) can be solved, which gives the following expressions for A', B', and C':

$$\begin{aligned} A' &= (16\langle\langle E^4 \rangle\rangle - 16m^2\langle\langle E^2 \rangle\rangle + 3m^4)n/3 , \\ B' &= (8\langle\langle E^4 \rangle\rangle - 11m^2\langle\langle E^2 \rangle\rangle + 3m^4)n/15 , \\ C' &= (\langle\langle E^4 \rangle\rangle - 2m^2\langle\langle E^2 \rangle\rangle + m^4)n/15 . \end{aligned} \quad \text{(B12)}$$

Once again, only one new coefficient $\langle\langle E^4 \rangle\rangle$ must be calculated in order to determine the whole tensor. For massless bosons, direct integration over the particle distribution yields

$$\langle\langle E^4 \rangle\rangle = \frac{360\zeta(7)}{\zeta(3)} T^4 . \quad \text{(B13)}$$

Let us now calculate the parameter δ defined in Eq. (A9) for a fluid in uniform motion along the x axis, with four-velocity $u^\mu \equiv (\sqrt{1+u^2}, u, 0, 0)$. The $y \to -y$ symmetry allows one to write

$$\begin{aligned} \langle p_T^4 \rangle &= \langle p_x^4 \rangle + \langle p_y^4 \rangle + 2\langle p_x^2 p_y^2 \rangle \\ &= (S^{11110} + S^{22220} + 2S^{11220})/(nu^0) . \end{aligned} \quad \text{(B14)}$$

Using Eqs. (B8) and (B12), this becomes, for massless particles,

$$\langle p_T^4 \rangle = (10u^4 + 8u^2 + 1)\frac{8\langle\langle E^4 \rangle\rangle}{15} . \quad \text{(B15)}$$

Note that, for a fluid at rest, the distribution is isotropic

and one gets directly $\langle p_T^4 \rangle = \langle \sin^4\theta \rangle \langle\langle E^4 \rangle\rangle = \frac{8}{15} \langle\langle E^4 \rangle\rangle$, in agreement with Eq. (B15). δ can now be calculated for massless bosons using Eqs. (4.13), (B15), and (B13):

$$\delta = \frac{3\zeta(7)\zeta(3)}{\zeta(5)^2} \frac{10u^4+8u^2+1}{(3u^2+1)^2} . \tag{B16}$$

It is minimal for $u=0$ and maximal for $u^2=\frac{1}{2}$ so that, for any value of u,

$$3.38 < \delta < 4.06 \tag{B17}$$

for massless bosons. For massless fermions, these bounds must be multiplied by $\frac{21}{25}$. Since Eq. (B17) is valid for all values of the fluid velocity, it can be used to estimate the finite multiplicity fluctuations in a hydrodynamic model.

[1] M. Gyulassy, K. A. Frankel, and H. Stöcker, Phys. Lett. **110B**, 185 (1982).
[2] H. A. Gustafsson *et al.*, Phys. Rev. Lett. **52**, 1590 (1984).
[3] G. Buchwald *et al.*, Phys. Rev. C **28**, 2349 (1983).
[4] J. Stachel, Nucl. Phys. **A525**, 23c (1991).
[5] B. Jacak, Nucl. Phys. **A525**, 77c (1991).
[6] J. D. Bjorken, Phys. Rev. D **27**, 140 (1983).
[7] P. Danielewicz and M. Gyulassy, Phys. Lett. **129B**, 283 (1983).
[8] L. D. Landau, Izv. Akad. Nauk SSSR **17**, 51 (1953).
[9] G. Baym, B. L. Friman, J.-P. Blaizot, M. Soyeur, and W. Czyz, Nucl. Phys. **A407**, 541 (1983).
[10] J.-P. Blaizot and J.-Y. Ollitrault, in *Quark-Gluon Plasma,* edited by R. C. Hwa (World Scientific, Singapore, 1990).
[11] F. Cooper and G. Frye, Phys. Rev. D **10**, 186 (1974).
[12] J.-Y. Ollitrault (unpublished).
[13] X.-N. Wang and R. C. Hwa, Phys. Rev. D **35**, 3409 (1987).
[14] J.-Y. Ollitrault, Phys. Lett. B **273**, 32 (1991).
[15] A. Kaidalov, Nucl. Phys. **A525**, 39c (1991), and references therein.
[16] F. Cooper, G. Frye, and E. Schonberg, Phys. Rev. D **11**, 192 (1975).
[17] E. V. Shuryak, Phys. Rep. C **61**, 72 (1980).
[18] H. von Gersdorff, L. McLerran, M. Kataja, and P. V. Ruuskanen, Phys. Rev. D **34**, 794 (1986); J.-P. Blaizot and J.-Y. Ollitrault, Phys. Lett. B **191**, 21 (1987).

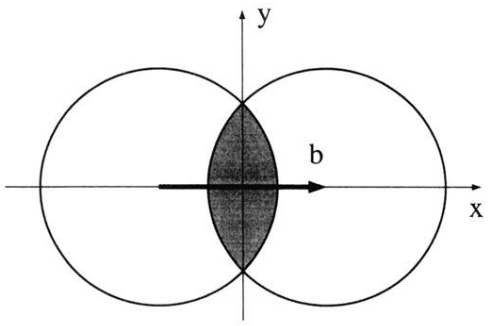

FIG. 1. Peripheral collision viewed in the transverse plane. **b** is the impact parameter. The shaded area corresponds to the region where particles are created in the central rapidity region. Outside this region is the vacuum.